Gas-Liquid Flow and Coalescence Characteristics of Bubbles in Expansion Microchannel

Zhang, Yuqi; Guo, Heng; Zhu, Chunying*[+]; Fu, Taotao; Ma, Youguang*[+]

State Key Laboratory of Chemical Engineering, School of Chemical Engineering and Technology, Tianjin University, Tianjin 300072, P.R. CHINA

ABSTRACT: *The flow behavior of bubbles in the expansion of the microchannel is studied. Four stable flow patterns are observed: Double-Layer-Bubble Coalescence (DLBC), Hamburger-Double-Layer-Bubble Coalescence (HDLBC), Hamburger Flow Coalescence (HFC), and Non-Coalescence Hamburger Flow (NCHF). With the increase of gas velocity, the flow pattern changes gradually from DLBC to HDLBC, HFC, and UHFC. The experimental results show that the liquid film drainage time increases with the bubble length. The location of bubble coalescence is away from the inlet with the increase of bubble length and bubble velocity but moves towards the inlet with the increase of liquid slug length. A prediction equation of bubble coalescence position is proposed, which has a good prediction effect.*

KEYWORDS*: Microchannel; Expansion channel; Bubble; Coalescence; Flow pattern.*

INTRODUCTION

The intelligent and green manufacturing based on informatization, automation, high efficiency, flexibility, and environmental friendliness has been the core development direction of the manufacturing industry. The traditional chemical industry is challenged due to its low efficiency, large equipment. Microfluidic technology is an emerging technology to process or manipulate small amounts of fluids at microliter levels using microchannel with tens to hundreds of micrometers [1], which is widely used in chemical synthesis [2], fluid mixing [3-6], cell sorting [7] and other fields. Compared with traditional methods, microfluidic technology has the advantages of low cost, less sample consumption, a high degree of automation, rapid and flexible operation, and miniaturization. Due to the wide application of bubbles in the fields of composite foam [8], atomic crystals [9], particle preparation [10] and cell encapsulation [11-14], the gas-liquid two-phase microreactor has attracted extensive attention [15-17]. The investigation of bubble coalescence has gained more interest because it diminishes the interfacial area between gas and liquid, and then affects the interphase mass transfer, performance of materials, and so forth.

The microchannel reactor is a miniaturized continuous flow pipeline reactor, which is manufactured through precision processing technology. In practical applications, the parallel multi-channel microreactor is widely used, in which the expansion structure is included before the outlet. The monodispersity of bubbles could be seriously destroyed by the coalescence of bubbles in the expansion structure. The bubbles/droplets are not only driven by the differential pressure during flow but also by the space squeezing of the confined channel, which can impact heat,

***** *To whom correspondence should be addressed.*
+ *E-mail: zhchy971@tju.edu.cn ; ygma@tju.edu.cn*
1021-9986/2023/1/181-191 11/$/6.01

mass and reaction processes [18]. To avoid the coalescence of bubbles in the gas-liquid two-phase process, it is of great significance to investigate the dynamic behavior and coalescence mechanism of bubbles in the expansion microchannel.

At present, a large of scholars have studied the coalescence of droplets/bubbles in microchannels with different configurations. *Yang et al.* [19] studied the coalescence process of bubbles in microchannels and found that the coalescence process of bubbles in the restricted microchannel was faster than that in unrestricted space due to the limitation of wall on bubbles. *Gunes et al.* [20] set many vertical channels on both sides of the main channel to drain the continuous phase from the main channel, which accelerated the liquid film drainage and realized the controllable droplet coalescence. Subsequently, *Wu et al.* [21] studied the coalescence behavior of bubbles in a T-shaped microchannel. The results show that the coalescence efficiency decreases with the increase of the apparent velocity of the two phases for both collision and extrusion coalescences. For expansion structure, *Tan et al.* [22] designed three channels with different structures, including rectangular expansion, tapered expansion and added branches. The length and width of the expansion structure and the velocity of the two-phase flow rate have important effects on the coalescence of droplets. In the microchannel with a conical expansion structure, many subsequent droplets coalesce due to the rapid decrease of droplet velocity and the discharge of the continuous phase. Different from the previous two structures, the microchannel with branches was used to control the droplet collision at the intersection to control the drainage time of the liquid film. Moreover, *Fu et al.* [23] experimentally studied the coalescence of bubbles in a microfluidic expansion device. Two different mechanisms of bubble coalescence were observed, moreover, three different bubble coalescence behaviors were proposed and analyzed. *Liu et al.* [24] studied the droplet coalescence at microchannel intersection chambers with different shapes and analyzed the coalescence location, coalescence time and critical conditions of coalescence. Finally, the coalescence behavior was analyzed. The study by *Anthony et al.* [25] showed that when two liquid droplets slowly gathered together, the tiny liquid neck or bridge was formed between them, and the expansion of the neck could be controlled by Laplace pressure. However, studies on droplet/bubble behavior and coalescence mechanism in the expansion structure of microreactors are still lacking, and need further research.

This paper constructs the expansion structure in a microchannel to investigate the bubble coalescence behavior. A high-speed digital camera was used to observe and record the bubble coalescence process visually. The effect of the two-phase flow rate on the flow pattern and coalescence characteristic of the bubbles in the swelling structure is systematically explored. A predictive model of the bubble, coalescence position is proposed, which helps to manipulate the bubble behavior and the design of the microreactor.

EXPERIMENTAL SECTION

Microfluidic equipment

The microchannel was milled on a polymethyl methacrylate (PMMA) plate and sealed with the other PMMA plate of the same size. The microchannel is shown in Fig. 1. In this paper, the microchannel consists of two parts: the forming part of the bubble and the expansion structure. The ionic liquid, 1-Butyl-3-methylimidazolium tetrafluoroborate ([Bmim][BF_4]) and N_2 were injected into the microchannel by two micro-injection pumps (Harvard Apparatus, PHD2000, USA, error 1%) to generate stable bubbles at T-junction. Bubbles flow through a straight microchannel of 20 mm and then enter the expansion structure with a width to depth ratio of 1:5 and a length of 10 mm. The cross-sections of the inlet channel and the main channel are 400 μm × 400 μm, and the channel depth of the expansion structure is 400 μm. All experiment was conducted at 298K and atmospheric pressure.

Experimental device and process

The experimental device is composed of three parts: microchannel equipment, flow control system and image acquisition system, as shown in Fig. 2. The microchip was placed horizontally on the platform of an inverted microscope (ECLIPSE Ti-CU, Nikon, Japan). A high-speed camera (Fastcam SA1.1, Japan) was installed on the microscope to observe and recorded the two-phase flow process in real-time. A 100 W halogen lamp (12 VDC) was used to illuminate the microchip. The inlet of the microchannel was connected to a 50 mL syringe for the experiment through a polyethylene tube with an inner diameter of 1.02 mm. When the two-phase flow was adjusted,

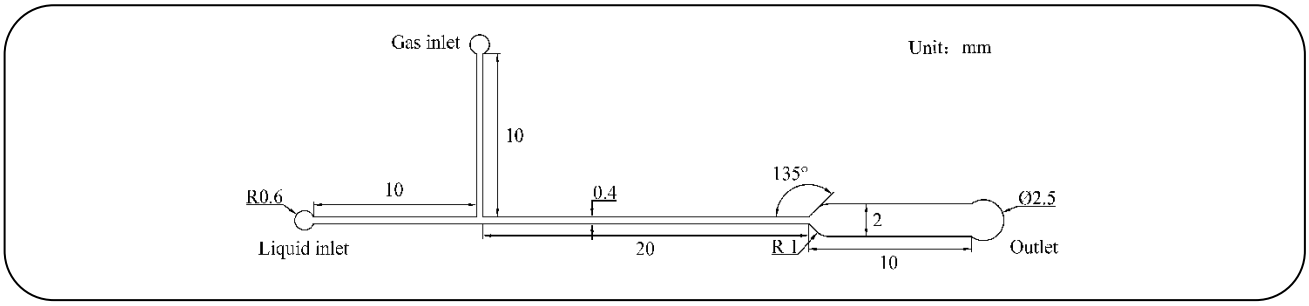

Fig. 1: Schematic diagram of the microchannel with expansion structure.

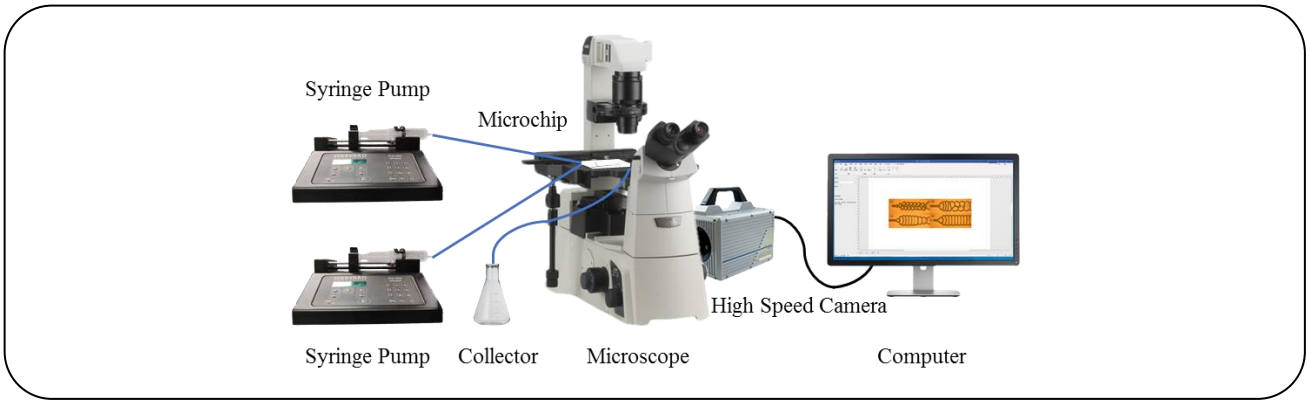

Fig. 2: Schematic diagram of the experimental procedure.

the bubbles inside the microchannel were recorded by the high-speed camera after the fluid flow reached a stable state for 5 minutes. Finally, using ImageJ software to analyze the recorded images. When the liquid film between two bubbles is drained away and two bubbles take place coalescence, the distance from the entrance of the expansion structure to the center of the coalesced bubble is defined as the coalescence distance of bubbles. The coalescence distance X and the length L for bubble or liquid slug could be obtained from images recorded by high-speed camera using image processing software. At least 20 images were processed, and the average value was used. The error of the coalescence distance X and the length L was evaluated to be 5 μm.

Fluid properties

The fluids used in the experiment are nitrogen (N_2) and ionic liquid. N_2 with a mass purity of ≥99% was purchased from Tianjin Hexi High-tech Gas Supply Station. Ionic liquid [BMIM][BF_4] (≥99.5 wt%) was purchased from Henan Lihua Pharmaceutical Co., Ltd. The density of the fluid was measured by a vibrating tube densitometer (Anton Paar MA-4500-M, Austria). The viscosity of the fluid was measured by a Ubbelohde viscometer (iVise, LAUDA. Germany). The interfacial tension between the two fluids was measured by the suspension drop method of a surface tensiometer (OCAH200, Data Physics instruments GmbH, Germany). The density of the liquid phase under the experimental conditions is 1201.5 kg·m^{-3}, the viscosity is 108.33 mPa·s, and the interfacial tension is 37.85 mN/m.

RESULTS AND DISCUSSION

Flow pattern

Contact and collision of bubbles are prerequisites for coalescence. *Bayareh et al.* [26] studied numerically the interaction between two drops in simple shear flow at finite Reynolds numbers (5≤ Re≤ 15), the results revealed that the collision mechanism includes three stages: Approach, collision, and separation. This phenomenon is usually caused by relative motion between the bubbles and the surrounding fluid [27]. With the change of gas-liquid two-phase flow velocity, four stable flow patterns were observed: Double-Layer-Bubble Coalescence (DLBC), Hamburger-Double-Layer-Bubble Coalescence (HDLBC), Hamburger Flow Coalescence (HFC), and Non-Coalescence Hamburger Flow (NCHF) (Fig. 3). Additionally, an unstable flow pattern was also observed, showing a periodic transformation between DLBC and HFC.

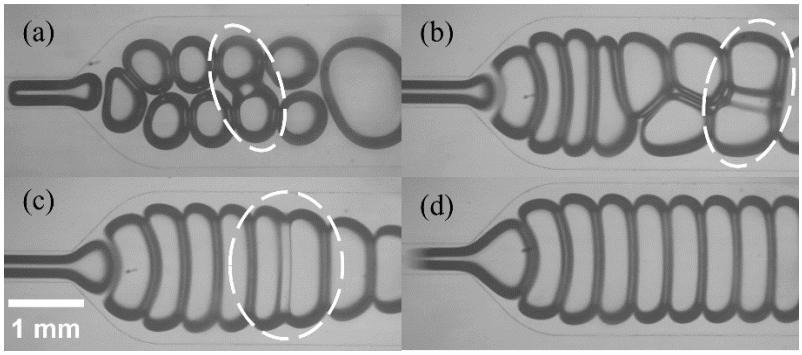

Fig. 3: The typical image of bubble coalescence flow pattern. (a) Double-layer-bubble coalescence (DLBC) (Q_G = 40 mL/h, Q_L = 40 mL/h), (b) Hamburger-double-layer-bubble coalescence (HDLBC) (Q_G = 40 mL/h, Q_L = 160 mL/h), (c) Hamburger flow coalescence (HFC) (Q_G = 40 mL/h, Q_L = 220 mL/h), (d) Non-coalescence hamburger flow (NCHF) (Q_G = 40 mL/h, Q_L = 280 mL/h).

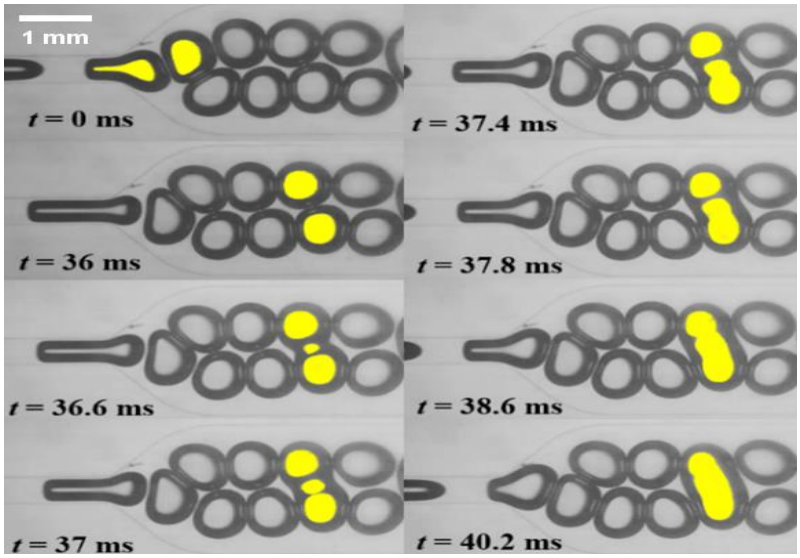

Fig. 4: Coalescence process of bubble for DLBC in the expansion structure (Q_G = 40 mL/h, Q_L = 20 mL/h).

Double-layer-bubble coalescence

The evolution diagram of bubble coalescence with time for DLBC is shown in Fig. 4. For a certain liquid phase flow rate, when the gas phase flow rate is low, the size of the bubbles generated at the T-junction is small. The bubbles enter the expansion structure, where they contact, squeeze and deform with each other. Under the action of the continuous phase, the bubbles flow in the form of a double-layer bubble flow in the expansion structure. Subsequently, the two adjacent bubbles coalesce. The evolution process of bubble coalescence can be divided into two stages: the squeezing and deformation stages. In the squeezing stage, from the moment when two bubbles touch each other in the expanding structure (t = 0 ms in Fig. 4) to the moment when coalescence occurs (t = 36.6 ms in Fig. 4). The change of bubble morphology was caused by the capillary force of the continuous phase and the squeezing pressure of the bubbles on the gas-liquid interface. Under the action of the capillary and squeezing forces, the liquid film between the two bubbles gradually becomes thinner until the liquid film ruptures and the two bubbles coalesce into one. In the deformation stage, from the moment when coalescence occurs (t = 36.6 ms in Fig. 4) to the moment when the bubbles form a stable ellipsoid (t = 40.2 ms in Fig. 4), the coalesced bubbles move forward and develop a flat shape under the action of surface tension.

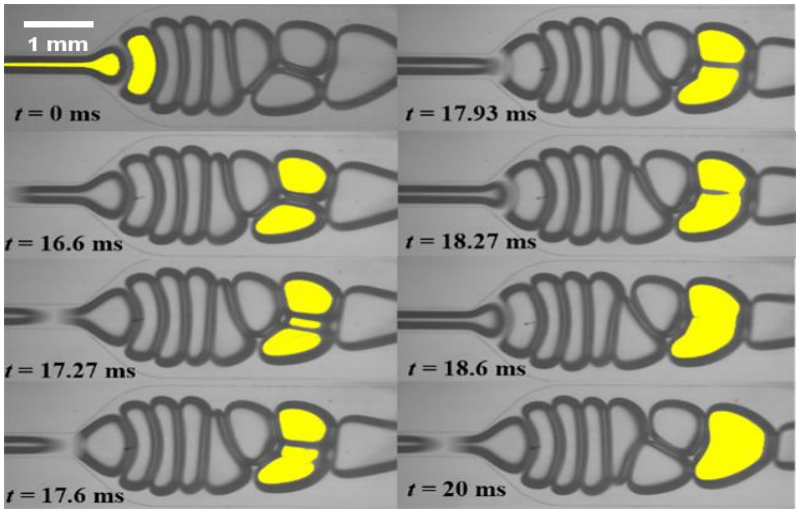

Fig. 5: Coalescence process of bubble for HDLBC in the expansion structure (Q_G= 180 mL/h, Q_L= 50 mL/h).

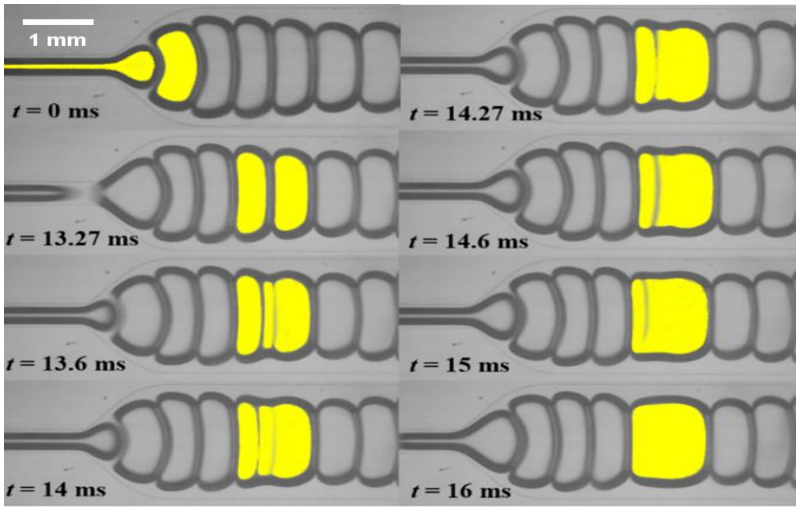

Fig. 6: Coalescence process of bubble for HFC in the expansion structure (Q_G=200 mL/h, Q_L=30 mL/h).

Hamburger-double-layer-bubble coalescence

With the increase of the gas flow rate, the size and flow velocity of bubbles generated at the T-junction gradually increase. The expansion structure causes the bubble flow velocity to drop sharply, and the bubbles flowing in front and back in the expansion structure are squeezed and deformed. In the process of flow along the axial direction of the channel, the bubble velocity gradually decreases until it stabilizes, and the squeezing force between the bubbles is correspondingly reduced. Under the action of surface tension, the bubble shape tends to a sphere, and the flow pattern transforms from the hamburger shape to the double-layer-bubble shape, and then coalescence occurs. The bubble coalescence process is similar to the DLBC process. It can be seen from Fig. 4 to Fig. 6 that this is a transitional flow pattern between the DLBC and the HFC.

Hamburger flow coalescence

With the further increase of the flow rate of the dispersed phase, the flow pattern transforms into the hamburger flow coalescence. Similar to the HDLBC, the bubbles entering the expansion structure squeeze each other, but the effect of surface tension is not enough to overcome the squeezing force to maintain the sphere. During the flow, the bubbles always maintain the shape of the hamburger. Similar to the DLBC, the evolution process

of bubble coalescence can be divided into two stages: the squeezing stage and the deformation stage. In the squeezing stage, from the moment when two bubbles touch each other in the expanding structure (t = 0 ms in Fig. 6) to the moment when coalescence occurs (t = 13.6 ms in Fig. 6), the liquid film between the two adjacent bubbles under the squeezing force is gradually drained away during the flow process, and then the two bubbles coalesce. The second stage is the deformation stage, the bubbles deform and form a stable ellipsoid after coalescence.

Non-coalescence hamburger flow

When the flow rate of the dispersed phase is higher, the contact area between two bubbles increases. Accordingly, the drainage time of liquid film increases. Simultaneously, the flow velocity of the bubble increases, resulting in a shorter residence time in the expansion structure. Therefore, no coalescence between bubbles takes place. As can be seen from Fig. 7, under the condition of this flow pattern, the bubbles present a uniform and stable hamburger flow in the expansion structure.

The type of bubble coalescence could be controlled by changing the flow rate of the continuous phase and the dispersed phase. Fig. 8 shows the gas-liquid two-phase flow patterns in the expansion structure. The unsteady flow pattern gradually disappears with the increase of liquid flow rate in the experimental conditions. Moreover, with the increase of the gas flow rate, the flow patterns present DLBC, HDLBC, HFC, NCHF, and unstable flow except for the low liquid flow rate (Q_L = 30 mL/h). Additionally, the gas flow rate for the transition of flow patterns elevates with the rise of the liquid flow rate.

Coalescence kinetics

DLBC, HDLBC and HFC are three stable coalescence flow patterns under experimental conditions. To avoid the coalescence behavior of bubbles in the expansion structure, it is very important to investigate the dynamic characteristics of these three coalescence flow patterns. Therefore, the drainage time of the liquid film and coalescence location of bubbles were studied.

Drainage time of the liquid film

Based on lubrication theory, a thinning equation of liquid film was derived from the Navier-Stokes equation and continuity equation by *Yang et al.* [19]. The drainage

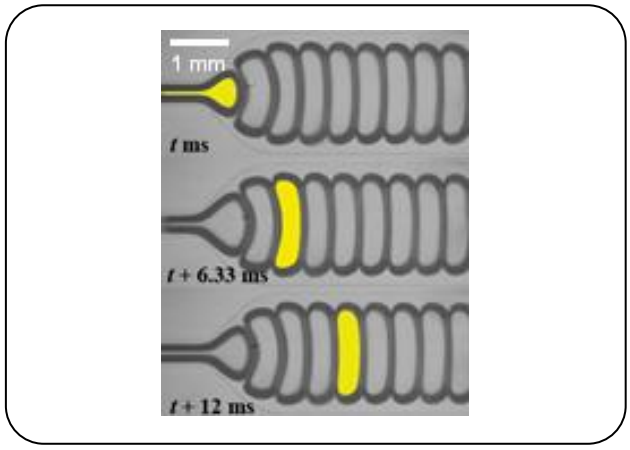

Fig. 7: Flow process of hamburger bubble in the expansion structure (Q_G=280 mL/h, Q_L=40 mL/h).

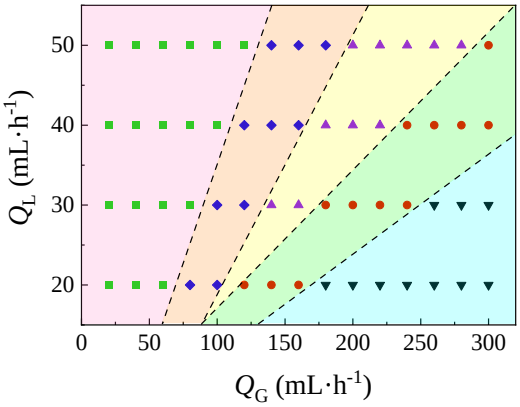

Fig. 8: Flow patterns of gas-liquid two-phase in expansion structure. ■: DLBC, ◆: HDLBC, ▲: HFC, ●: NCHF, ▼: unstable flow.

time can be obtained by integrating the thinning equation of liquid film. Although the confined space in the microchannel is micro-scale, the size of bubbles is much larger than the interface scale. Therefore, the liquid film drain model as a basic theory is still applicable to the bubble coalescence in the microchannel.

The relationship between microbubble length and two-phase flow rate is shown in Fig. 9(a). The bubble length increases with the increase of gas flow rate and decrease of liquid flow rate, correspondingly, the length of the liquid slug decreases (Fig. 9(b)). This is consistent with the results of *Garstecki et al.* [28]. With the increase of bubble length, the contact area between bubbles is increased, and thus it is more difficult to drain the liquid film, leading to the increase of the liquid film drainage time. The decrease in the length of the liquid slug could reduce the squeezing

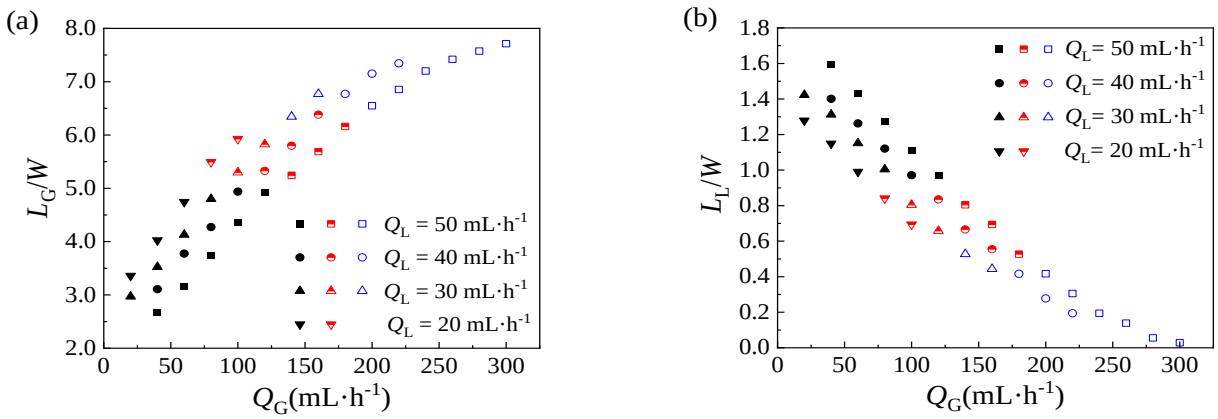

Fig. 9: Variation of (a) Ratio of bubble length to main microchannel width (b) Ratio of liquid slug length to main microchannel width with gas/liquid flow rate. Solid symbols: DLBC; half-solid symbols: HDLBC; hollow symbols: HFC.

force of the upstream liquid slug on the downstream bubbles. As a result, the drainage time of the liquid film extends [19].

Theoretically, the liquid film draining theory has been commonly recognized to elucidate the coalescence mechanism of bubbles. The initial thickness of liquid film between two bubbles relies primarily on the fluid properties (density, viscosity and interfacial tension), flow parameters (radius and velocity of droplets) and so on [29]. Due to the combined action of squeezing and capillary pressure, the liquid film could be gradually drained away. When the liquid film becomes thin sufficiently, Van der Waals force or other intermolecular forces would become important to cause film breakup and accordingly the bubbles coalescence. The time interval from contact of two bubbles to coalescence in the expansion structure was defined as the liquid film drainage time T. T is a predominated parameter to determine whether bubbles coalesce or not. As can be seen from Fig. 10(a), with the increase of bubble length, the liquid film drainage time increases. The larger the bubble length is, the larger the liquid film volume between bubbles is, and the more difficult it is to drain the liquid film, thus the longer the liquid film drainage time is [19, 30]. The inset diagram in Fig. 10(a) also supports this conclusion. It can be seen that when the gas flow rate increases or when the liquid flow rate decreases, the bubble size accordingly increases, and the liquid film drainage time gets longer. In traditional equipment, large bubbles are more likely to coalesce than small bubbles because of the high probability of collisions [30]. However, the bubble coalescence in this experiment is chasing and coalescing process in the restricted channel, showing an opposite result: the large bubbles are less likely to coalescence than small bubbles.

As can be seen from Fig. 10(b), with the increase of bubble length to liquid slug length ratio L_G/L_L, the liquid film drainage time increases correspondingly. With the increase of L_G/L_L, the size of bubbles increases, and then the contact area between bubbles increases, the liquid film drying time increases. Simultaneously, liquid slug length decreases, the squeezing force of the upstream fluid on bubbles accordingly reduces, leading to the extension of the liquid film drainage time. On the other hand, the reduction of the liquid slug length could make the liquid film thickness between bubbles thin, leading to a shrinkage of the liquid film drainage time. The liquid film drainage time increases with L_G or L_G/L_L, indicating the bubble size is predominant to liquid film drainage time. In addition, with the increase of L_G/L_L, the liquid film drainage time increases quickly and then tends to a constant. For a given liquid flow rate, the bubble size increases from swiftly to slowly with the gas flow rate (Fig. 9(a)). Thus the liquid film drainage time is increased quickly first and then slowly.

Coalescence distance of bubbles

The conclusion of the continuity equation points out that the velocity increases with the increase of the flow rate for the constant density liquid in a channel with a constant cross-sectional area. Fig. 11 exhibits the influences of the gas-liquid flow on X. When the gas flow rate increases, the drainage time of the liquid film and the bubble velocity increase, correspondingly, the bubble coalescence distance is farther. However, increasing the flow of liquid will limit

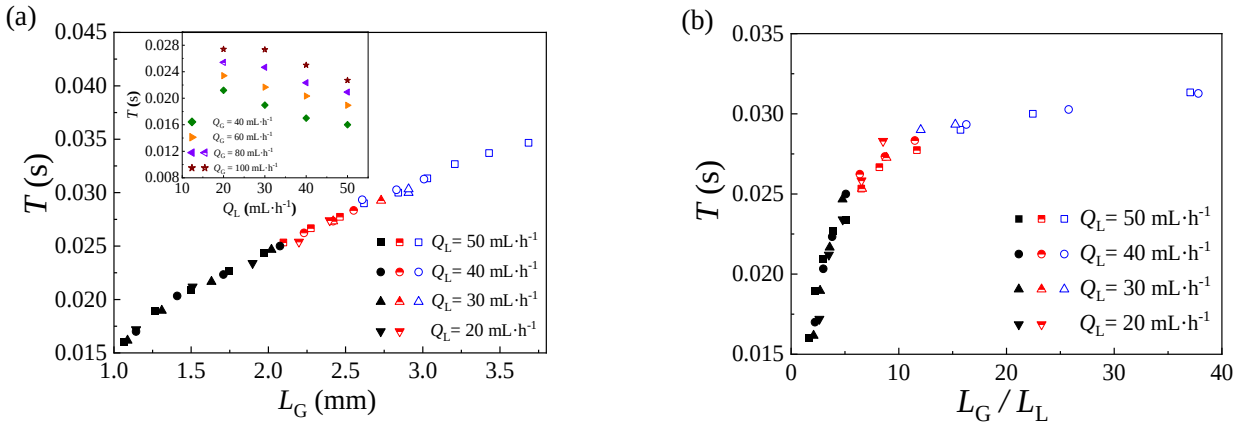

Fig. 10: Liquid film drainage time. (a) Effect of bubble size; (b) The ratio of bubbles to liquid slug length. Solid symbols: DLBC; half-solid symbols: HDLBC; hollow symbols: HFC.

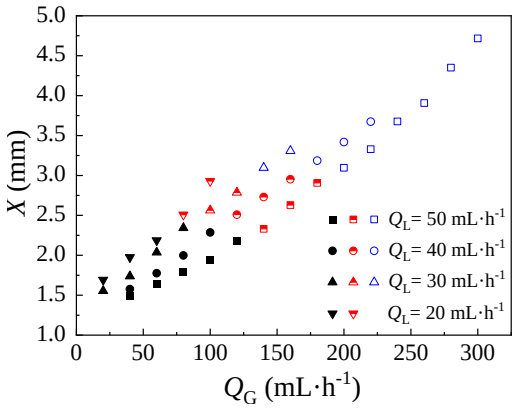

Fig. 11: Variation of coalescence distance of bubbles with gas or liquid flow rate. Solid symbols: DLBC; half-solid symbols: HDLBC; hollow symbols: HFC.

the growth of the bubble and the drainage time of the liquid film. Although the speed is increased, the bubble coalescence distance decreases.

It can be found from the above analysis, the coalescence distance of bubbles in the expansion structure is mainly affected by the liquid film drainage time and bubble velocity, which is correlative with the physical properties of fluids, gas or liquid flow rate and so on. Reynolds number, representing the ratio of inertia force to viscous force, was used to correlate the coalescence distance of bubbles in the expansion structure. Therefore, the coalescence distance of bubbles in expansion structure could be correlated by the following correlation:

$$X/W=A_1 Re_G^{A_2} Re_L^{A_3} \quad (1)$$

Where W is the width of the main channel. $Re_G = d_H \rho_G U_G / \mu_G$, $Re_L = d_H \rho_L U_L / \mu_L$, ρ, μ and U are the density, viscosity and apparent velocity of the fluids. $U_G = Q_G / W^2$, $U_L = Q_L / W^2$. d_H is the hydraulic diameter of the main channel. A_i (i = 1, 2, 3) is the fitting parameter, which could be obtained through experimental data. For the expansion structure in this work, A_1 = 2.9464, A_2 = 0.5683, A_3 = -0.3424. The comparison between experimental data and calculated values is shown in Fig. 12. The average deviation between calculated values by Equation (1) and experimental data is 6.9%, indicating good predicting performance. The research on the location of bubble coalescence can provide theoretical guidance for the industrial application of microchemical technology. Because of the understanding of the location of coalescence, the occurrence of coalescence can be effectively suppressed, and the effect of coalescence on the monodispersity of bubbles in the channel can be avoided, thereby ensuring efficient mass transfer or reaction in the microreactor.

CONCLUSIONS

The flow behavior of bubbles in a microchannel with an expansion structure was studied. Four stable flow patterns were observed: Double-Layer-Bubble Coalescence (DLBC), Hamburger-Double-Layer-Bubble Coalescence (HDLBC), Hamburger Flow Coalescence (HFC), and Non-Coalescence Hamburger Flow (NCHF). The coalescence distance of bubbles increases with the increase of gas flow rate or decrease of liquid flow rate. This phenomenon is related to the drain time of liquid film and bubble velocity.

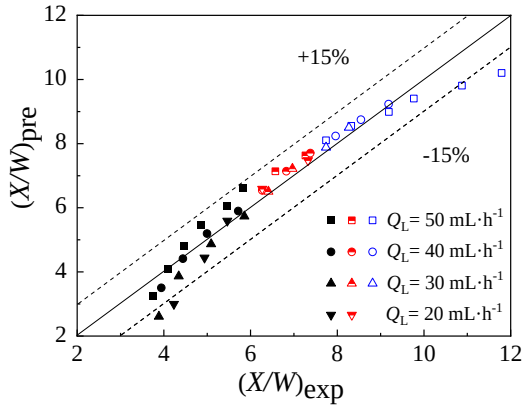

Fig. 12: Comparison of X/W between experimental data and calculated values. Solid symbols: DLBC; half-solid symbols: HDLBC; hollow symbols: HFC.

The larger the gas flow rate is, or the smaller the liquid flow rate is, the longer the bubbles are, the shorter liquid slugs are, accordingly leading to the increase of the liquid film drain time. With the increase of gas flow rate and liquid flow rate, the bubble velocity increases. Under the conjunct action of bubble velocity and drainage time, the coalescence distance of bubbles increases correspondingly. Considering the influence of operating conditions on coalescing position, a prediction equation of coalescence distance of bubbles was proposed with a good predicting performance. The results could provide support for the design and optimization in scale-up of microreactor to avoid the bubble coalescence. In this work, only one channel was designed and studied. The optimization of the expansion structure is also issues to be considered. Moreover, the coalescence mechanism and the influencing mechanism of bubble coalescence on the mass transfer and reaction are important to the development and optimization of microreactor.

Nomenclature

d_H	Hydraulic diameter of the main channel, m
L_G	Length of the bubble, m
L_L	Length of the liquid, m
Q_G	Flow rate of gas, m^3/s
Q_L	Flow rate of liquid, m^3/s
Re	Reynolds number, dimensionless
t	Time, s
T	Liquid film drainage time, s
U	Apparent velocity of the fluids m/s
W	Width of the main channel, m
X	Coalescence distance of bubbles, m

Greek Letters

ρ	Density of fluids, kg/m^3
μ	Viscosity of fluids, Pa·s
σ	Interfacial tension between two phases, mN/m

Subscripts

B	Bubble
G	Gas phase
L	Liquid phase

Acknowledgments

Supported by the National Natural Science Foundation of China (No. 21978197, 92034303).

Received : Nov. 5, 2021 ; Accepted : Feb. 14, 2022

REFERENCE

[1] Whitesides G.M., The Origins and the Future of Microfluidics, *Nature*, **442**: 368-373 (2006).

[2] Pasha M., Li G., Shang M., Liu S., Su Y., Mass Transfer and Kinetic Characteristics for CO_2 Absorption in Microstructured Reactors Using an Aqueous Mixed Amine, *Sep. Purif. Technol. (SPUTFP)*, **274**: 118987 (2021).

[3] Lv H., Chen X., New Insights Into the Mechanism of Fluid Mixing in the Micromixer Based on Alternating Current Electric Heating with Film Heaters, *Int. J. Heat Mass Transf. (IJHMAK)* **181**: 121902 (2021).

[4] Lv H., Chen X., Zeng X., Optimization of Micromixer with Cantor Fractal Baffle Based on Simulated Annealing Algorithm, *Chaos Solitons Fractals (CSFOEH)* **148**:111048 (2021).

[5] Lv H., Chen X., Wang X., Zeng X., Ma Y., A Novel Study on a Micromixer with Cantor Fractal Obstacle Through Grey Relational Analysis, *Int. J. Heat Mass Transf. (IJHMAK)* **183**:122159 (2021).

[6] Yu Q., Chen X., Insights Into the Breaking and Dynamic Mixing of Microemulsion (W/O) in the T-Junction Microchannel, *Chaos Solitons Fractals (CSFOEH)* **155**:111774 (2022).

[7] Tay A., Pfeiffer D., Rowe K., Tannenbaum A., Popp F., Strangeway R., Schuler D., Di Carlo D., High-Throughput Microfluidic Sorting of Live Magnetotactic Bacteria, *Appl. Environ. Microbiol. (AEMIDF)*, **84**: e01308-18 (2018).

[8] Vecchiolla D., Giri V., Biswal S.L., Bubble–Bubble Pinch-Off in Symmetric and Asymmetric Microfluidic Expansion Channels for Ordered Foam Generation, *Soft Matter (SMOABF)*, **14**: 9312-9325 (2018).

[9] Huang X., Li Z., Deng, Y., Cai W., Gu L., Lu H., Effect of Micro- and Nanobubbles on the Crystallization of THF Hydrate Based on the Observation by Atomic Force Microscopy, *J. Phys. Chem. C (JPCCCK)*, **124**: 13966-13975 (2020).

[10] Dedovets D., Li Q., Leclercq L., Nardello-Rataj V., Leng J., Zhao S., Pera-Titus M., Multiphase Microreactors Based on Liquid–Liquid and Gas–Liquid Dispersions Stabilized by Colloidal Catalytic Particles, *Angew. Chem.-Int. Edit.* (*ACIEF5*), 10.1002/anie.202107537 (2021).

[11] Choi C.H., Wang H., Lee H., Kim J.H., Zhang L., Mao A., Mooney D.J., Weitz D.A., One-Step Generation of Cell-Laden Microgels Using Double Emulsion Drops with a Sacrificial Ultra-Thin Oil Shell, *Lab Chip (LCAHAM)*, **16**: 1549-1555 (2016).

[12] Lee T.Y., Praveenkumar R., Oh Y.K., Lee K., Kim S.H., Alginate Microgels Created by Selective Coalescence between Core Drops Paired with an Ultrathin Shell, *J. Mat. Chem. B (JMCBDV)*, **4**: 3232-3238 (2016).

[13] Shen Y., Hu L., Chen W., Xie H., Fu, X., Drop Encapsulated in Bubble: A New Encapsulation Structure, *Phys. Rev. Lett. (PRLTAO)*, **120**: 054503 (2018).

[14] He M., Edgar J.S., Jeffries G.D.M., Lorenz R.M., Shelby J.P., Chiu D.T., Magnetic Targeting and Ultrasound Activation of Liposome-Microbubble Conjugate for Enhanced Delivery of Anticancer Therapies, *ACS Appl. Mater. Interfaces (AAMICK)*, **12**: 23737-23751 (2020).

[15] Deng N.N., Sun S.X., Wang W., Ju X.J., Xie R., Chu L.Y., A Novel Surgery-Like Strategy for Droplet Coalescence in Microchannels, *Lab Chip (LCAHAM)*, **13**: 3653-3657 (2013).

[16] Chen J.S., Jiang J.H., Droplet Microfluidic Technology: Mirodroplets Formation and Manipulation, *Chin. J. Anal. Chem. (FHHHDT)*,**40**: 1293-1300 (2012).

[17] Xiao Z., Zhang B., Droplet Microfluidics: Technologies and Applications, *Chin. J. Chromatogr. (SEPUER)*, **29**: 949-956 (2011).

[18] Bayareh M., Mortazavi S., Three-Dimensional Numerical Simulation of Drops Suspended in Simple Shear Flow at Finite Reynolds Numbers, *Int. J. Multiph. Flow (IJMFBP),s* **37**: 1315-1330 (2011).

[19] Yang L., Wang K., Tan J., Lu Y., Luo G., Experimental Study of Microbubble Coalescence in a T-junction Microfluidic Device, Microfluid. Nanofluid, *Microfluid. Nanofluid. (MNIAAR)*, **12**: 715-722 (2012).

[20] Gunes D.Z., Bercy M., Watzke B., Breton O., Burbidge A.S., A Study of Extensional Flow Induced Coalescence in Microfluidic Geometries with Lateral Channels, *Soft Matter (SMOABF)*, **9**: 7526-7537 (2013).

[21] Wu Y., Fu T., Zhu C., Ma Y., Li H.Z., Bubble Coalescence at a Microfluidic T-Junction Convergence: from Colliding to Squeezing, *Microfluid. Nanofluid. (MNIAAR)*, **16**: 275-286 (2014).

[22] Tan Y.C., Fisher J.S., Lee A.I., Cristini V., Lee A.P., Design of Microfluidic Channel Geometries For The Control of Droplet Volume, Chemical Concentration, and Sorting, *Lab. Chip. (LCAHAM)*, **4**: 292-298 (2004).

[23] Fu T., Ma Y., Li H.Z., Bubble Coalescence In Non-Newtonian Fluids in a Microfluidic Expansion Device, *Chem. Eng. Process. (CENPEU)*, **97**: 38-44 (2015).

[24] Liu Z., Wang X., Cao R., Pang Y., Droplet Coalescence at Microchannel Intersection Chambers with Different Shapes, *Soft Matter (SMOABF)*, **12**: 5797-5807 (2016).

[25] Anthony C.R., Harris M.T., Basaran O.A., Initial Regime of Drop Coalescence, *Phys. Rev. Fluids (PLEEE8)*, **5**: 033608 (2020).

[26] Bayareh M., Mortazavi S., Binary Collision of Drops in Simple Shear Flow at Finite Reynolds Numbers: Geometry and Viscosity Ratio Effects, *Adv. Eng. Softw*. **42**: 604-611 (2011).

[27] Liao Y.X.; Lucas D., A Literature Review of Theoretical Models for Drop and Bubble Breakup in Turbulent Dispersions, *Chem. Eng. Sci. (CESHAR)* **64**: 3389–3406 (2009).

[28] Garstecki P., Fuerstman M.J., Stone H.A., Whitesides G.M., Formation of Droplets and Bubbles in a Microfluidic T-Junction-Scaling and Mechanism of Break-Up, *Lab Chip (LCAHAM)*, **6**: 437-446 (2006).

[29] Chesters A.K., The Applicability of Dynamic-Similarity Criteria to Isothermal, Liquid-Gas, Two-Phase Flows Without Mass Transfer, *Int. J. Multiph. Flow (IJMFBP)* **2**: 191-212 (1975).

[30] Tsang Y.H., Koh Y.H., Koch D.L., Bubble-Size Dependence of the Critical Electrolyte Concentration for Inhibition of Coalescence, *J. Colloid Interface Sci. (JCISA5)*, **275**: 290-297 (2004).